Global Nitrogen and Sulfur Deposition Mapping Using a Measurement-Model Fusion Approach

Hannah J. Rubin[1], Joshua S. Fu[1,2], Frank Dentener[3], Rui Li[4], Kan Huang[5], Hongbo Fu[5]

[1]Department of Civil and Environmental Engineering, University of Tennessee, Knoxville, TN, 37996, USA

[2]Computational Earth Science Group, Oak Ridge National Laboratory, Oak Ridge, TN 37831, USA

[3]European Commission, Joint Research Centre, Sipra, Italy

[4]Ministry of Education Key Laboratory for Earth System Modeling, Department of Earth System Science, Tsinghua University, Beijing, 100084, China

[5]Shanghai Key Laboratory of Atmospheric Particle Pollution and Prevention (LAP3), Department of Environmental Science and Engineering, Fudan University, Shanghai, 200433, China

E-mail: jsfu@utk.edu

Keywords: Measurement-model fusion, nitrogen deposition, sulphur deposition, HTAP II, ammonia, multiple-model mean

Abstract

Global reactive nitrogen (N) deposition has more than tripled since 1860 and is expected to remain high due to food production and fossil fuel consumption. Global sulfur emissions have been decreasing worldwide over the last 30 years, but many regions are still experiencing unhealthily high levels of deposition. We update the 2010 global deposition budget for reactive nitrogen and sulfur components with new regional wet deposition measurements from Asia, improving the ensemble results of eleven global chemistry transport models from the second phase of the United Nation's Task Force on Hemispheric Transport of Air Pollution (HTAP-II). The observationally adjusted global N deposition budget is 114.5 Tg-N, representing a minor increase of 1 % from the model-only derived values, and the adjusted global sulfur deposition budget is 88.9 Tg-S, representing a 6.5% increase from the modelled values, using an interpolation distance of 2.5 degrees. Regionally, deposition adjustments can be up to ~73% for nitrogen, and 112% for sulfur. Our study demonstrates that a global measurement-model fusion approach can improve N and S deposition model estimates at a regional scale, with sufficient availability of observations, but in large parts of the world, alternative approaches need to be explored. The analysis presented here represents a step forward toward the World Meteorological Organization's goal of global fusion products for accurately mapping harmful air pollution deposition.

1. Introduction

Atmospheric nitrogen and sulfur deposition from human activities related to the use of fossils and land use have significant implications for ecosystem and human health. Elevated levels of nitrogen and sulfur can lead to eutrophication (Anderson et al., 2008; Heisler et al., 2008), changes in carbon sequestration (Kicklighter et al., 2019; de Vries et al., 2009; Zhu et al., 2020), loss of biodiversity (Clark et al., 2013; Dise and Stevens, 2005), and acidification (Bowman et al., 2008). While sulfur deposition is expected to decrease over the next 80 years (Lamarque et al., 2013), it will remain a serious hazard in many emerging economies. For instance, sulfur deposition in East Asia peaked in 2006 (Lu et al., 2010) but is still high enough to be concerning, especially in natural and semi-natural regions (Doney et al., 2007; Luo et al., 2014).

Oxidized nitrogen (NO_y) and reduced nitrogen (NH_x), together called reactive nitrogen (Nr), and oxidized sulfur (SO_x) deposition occur as wet and dry processes (Dentener et al., 2006). Wet deposition is measured at hundreds of locations in Europe, North America, and Asia, but dry deposition is harder to measure and is often instead derived from ambient concentrations and modeled deposition velocities (Xu et al., 2015). For example, dry deposition is inferred from continuous concentration measurements combined with modeled dry deposition velocities at a few locations in North America (Clean Air Status and Trends Network (CASTNET), 2021) and Asia (Acid Deposition Monitoring Network in East Asia (EANET), 2021).

The United Nations Economic Commission for Europe's Task Force on Hemispheric Transport of Air Pollution (HTAP) is an international effort to improve the understanding of air pollution transport science with emissions models. The second phase of HTAP was launched in 2012. Tan et al. (2018) used the multi-model mean (MMM) of 11 HTAP II chemistry transport models to estimate the sulfur and nitrogen deposition budgets for 2010. Significant uncertainty remained due to a lack of station measurements, especially in East Asia, a large contributor to the overall budget. Tan et al. (2018) compared Acid Deposition Monitoring Network in East Asia (EANET (Acid Deposition Monitoring Network in East Asia, 2021)) measurements to the MMM output but there were very few measurements in East Asia and all were located along the southeastern coast. In contrast, the highest emissions and modeled deposition were inland and north, making it challenging to evaluate model performance.

Combining measurements and model estimates in a "measurement-model fusion" (MMF) approach has the advantage of retaining the broad spatial coverage of models while accurately matching observations. Generally speaking, MMF takes model estimates of concentrations or fluxes for a region and modifies them based on in-situ point measurements to force the model towards the observed values (Labrador et al., 2020). One global MMF approach for wet deposition combined measurements with HTAP I ensemble model values for 2000-2002 (Vet et al., 2014) where model estimates filled empty grid cells lacking a 3-year observed mean. Another MMF approach in North America (Atmospheric Deposition Analysis Generated from optimal Interpolation from Observations, "ADAGIO") used observed concentrations to adjust predicted concentrations from the Global Environmental Multiscale-Modelling Air Quality and Chemistry (GEM-MACH) model (Schwede et al., 2019). Recent work in the US (Schwede and Lear, 2014; Zhang et al., 2019) incorporates Community Multiscale Air Quality (CMAQ) model

output and precipitation data generated by the Parameter-elevation Regressions on Independent Slopes Model (PRISM, https://prism.oregonstate.edu/, Accessed: 10/01/22), as well as observations using inverse distance weighting to create total deposition ("TDep", https://nadp.slh.wisc.edu/committees/tdep/#tdep-maps) maps that are publicly available.

More details of the MMF approach are described in Fu et al. (2022) as they lay out a roadmap for future work, following the World Meteorological Organization's Global Atmosphere Watch Program (WMO GAW) and the intended role of the MMF Global Total Atmospheric Deposition (MMF-GTAD) project. This study updates Tan et al.'s (2018) global S and N deposition budgets using a variation of the TDep methodology (Schwede and Lear, 2014) to merge NH_x, NO_y, and SO_x modelled gridded deposition fluxes results with deposition fluxes derived from observations of NO_3^-, NH_4^+, and SO_4^{2-} in precipitation and precipitation amounts The main purpose of our study is to demonstrate the viability of a straightforward but globally applicable MMF approach, while remaining consistent with previous work that provided datasets for impact assessments for various communities. This approach is an important intermediate step towards the WMO's goal of reliable deposition products to aid decision-making. We update the 2010 deposition budgets using MMF to combine the broad spatial coverage of a model with accurate in-situ measurements.

2. Data Availability

Table 1: Sources of deposition observations.

Name	Source	Number of Observation Sites	Region	Value
NTN, AIRMoN	NADP	247	USA	wet deposition
CASTNET	NADP	84	USA	dry deposition
CAPMoN	NAtChem	27	Canada	wet and dry deposition
EMEP	EMEP	86	Europe	wet deposition
China Scientific Study	Li et al. 2019	407	China	wet deposition

EANET	EANET	47	East Asia	wet and dry deposition
IDAF	INDAAF	1	Niger	wet deposition

All data are from 2010, reported monthly with sources summarized in Table 1. Wet deposition measurements (NO_3^-, NH_4^+, and SO_4^2) from the US's National Trends Network (NTN) and Atmospheric Integrated Research Monitoring Network (AIRMoN) are available through the National Atmospheric Deposition Program (NADP (National Atmospheric Deposition Program, 2021), http://nadp.slh.wisc.edu/NTN/). Measurements were filtered for completeness and quality, following Schwede and Lear (2014). Sites without a full year of measurements or with quality tags indicating collection issues were not included, resulting in 247 observations in the US. Dry deposition generated values are available from the Clean Air Status and Trends Network (CASTNET, 2021) at 84 locations. CASTNET uses an inferential method to calculate dry deposition fluxes as a product of surface concentration and modeled dry deposition velocity. Nitrogen and sulfur wet deposition measurements and dry deposition estimates throughout Canada are recorded by the Canadian Air and Precipitation Monitoring Network (CAPMoN (2021) and are available through the National Atmospheric Chemistry (NAtChem) database (https://donnees.ec.gc.ca/data/air/monitor/). Dry deposition estimates from CAPMoN are calculated by multiplying atmospheric concentration and deposition velocity. There were 27 sites with a full year of quality checked data for 2010.

The European Monitoring and Evaluation Programme (EMEP (European Monitoring and Evaluation Prgrarmme (EMEP), 2021; Tørseth et al., 2012), http://ebas-data.nilu.no/) provides records of precipitation chemistry (NO_3^-, NH_4^+, and SO_4^{2-}) and precipitation depths for Europe. There were 86 sites with a full year of quality checked data in 2010.

In China, a multi-year nationwide field study, including some of these NNDMN data, was compiled by Li et al. (2019). Daily NO_3^-, NH_4^+, and SO_4^{2-} site measurements (in mg/L) were averaged for 2010 for each of the 407 site locations with complete records by multiplying the concentration by the precipitation recorded at that same site (in mm) and then aggregating to produce annual precipitation-weighted deposition (Sirois, 1990). For a wider Asian region,

EANET (Asia Center for Air Pollution Research, 2021, https://www.eanet.asia/) wet and dry deposition and precipitation data are available at 47 sites.

The International Global Atmospheric Chemistry (IGAC) Deposition of Biogeochemically Important Trace Species (DEBITS) Africa (IDAF) program (Adon et al., 2010; Galy-Lacaux et al., 2014) has NH_4^+ and NO_3^- precipitation concentrations on the International Network to Study Deposition and Atmospheric Chemistry in Africa (INDAAF (INDAAF – International Network to study Deposition and Atmospheric chemistry in AFrica, 2021)) website (https://indaaf.obs-mip.fr/) for one site in Niger. All measurements were converted to mg-N (or S) /m^2/yr.

3. Measurement Model Fusion Procedure

Global yearly wet and dry NO_3^-, NH_4^+, and SO_4^{2-} deposition observations (for wet deposition) or estimates derived from near-surface concentrations and modelled deposition velocities for dry deposition) were combined with the respective HTAP II model average grid cell estimates, using model output interpolated to common 1 degree x 1 degree (1º x 1º) grid cells (Figure 1). For example, wet NO_3^- deposition observations are combined with the wet NO_3^- modeled deposition in the nearest HTAP II MMM grid cell to the observation, where observations exist. Dry deposition values (NO_3^-, NH_4^+, and SO_4^{2-}) from CASTNET and an inverse-distance weighted 1º x 1º gridded dataset was created based on the distance from each observation to the center of the nearest HTAP II model grid cell. Inverse-distance weighting (IDW) was selected as the most straight forward to implement method to introduce MMF on a global scale while remaining consistent with previous work (Schwede and Lear, 2014).

The weighting function was calculated as

$$\left(1 - \frac{distance}{max\ distance}\right)^2 \quad (1)$$

following Schwede and Lear's (Schwede and Lear, 2014) approach for the TDep product, where "distance" is the distance between the site location and the center of the HTAP II model grid cell nearest to that sampling site location, within a maximum distance of 2.5º (approximately 280 km at middle latitudes). The choice of the maximum distance is a crucial parameter for the inverse distance weighting method in MMF. Prior analysis (e.g. Tan et al. 2018b) has shown that gaseous and particulate sulfur and nitrogen emissions can travel several hundreds of kilometers,

before being deposited, although there is likely to be a large variation of transport distances due to regional differences in chemistry, meteorological conditions, transport patterns and removal processes. These processes interact with spatially heterogeneous emissions. Since there will not be a single distance that captures the heterogeneity of all processes at play, we present here a base case using a 2.5º interpolation distance, and two sensitivity cases reducing the distance to 1º and increasing it to 5º, respectively. The 5º distance can be seen as an upper limit for the distance where deposition observations can constrain deposition. The output values of the weighting function at each observation location are then multiplied by the observed deposition. For the center of every HTAP II model grid cell near that site, the modeled deposition is multiplied by 1 minus the value of the weighting function. Consequently, if there are no observations near the model grid cells, the cell value remains the same. The two grid values ([weighting function times observed deposition] and [1-weighting function times modeled deposition]) are added together to give the value of the MMF estimate. This has the effect of modifying the HTAP II grid values only in locations where there are observations within the maximum interpolation distance.

The MMF gridded surfaces were then summed by species along with the remaining unchanged HTAP II gridded surfaces that lacked in-situ measurements to create total N and S deposition gridded surfaces (e.g., the MMF wet and dry SO_4^- gridded surfaces were added to the HTAP II wet and dry SO_2 gridded surfaces to get total S deposition). The MMF wet deposition surfaces include measurements from Europe, Asia, and North America, and the dry deposition MMF surfaces include estimates from the USA and Asia (see section 2)

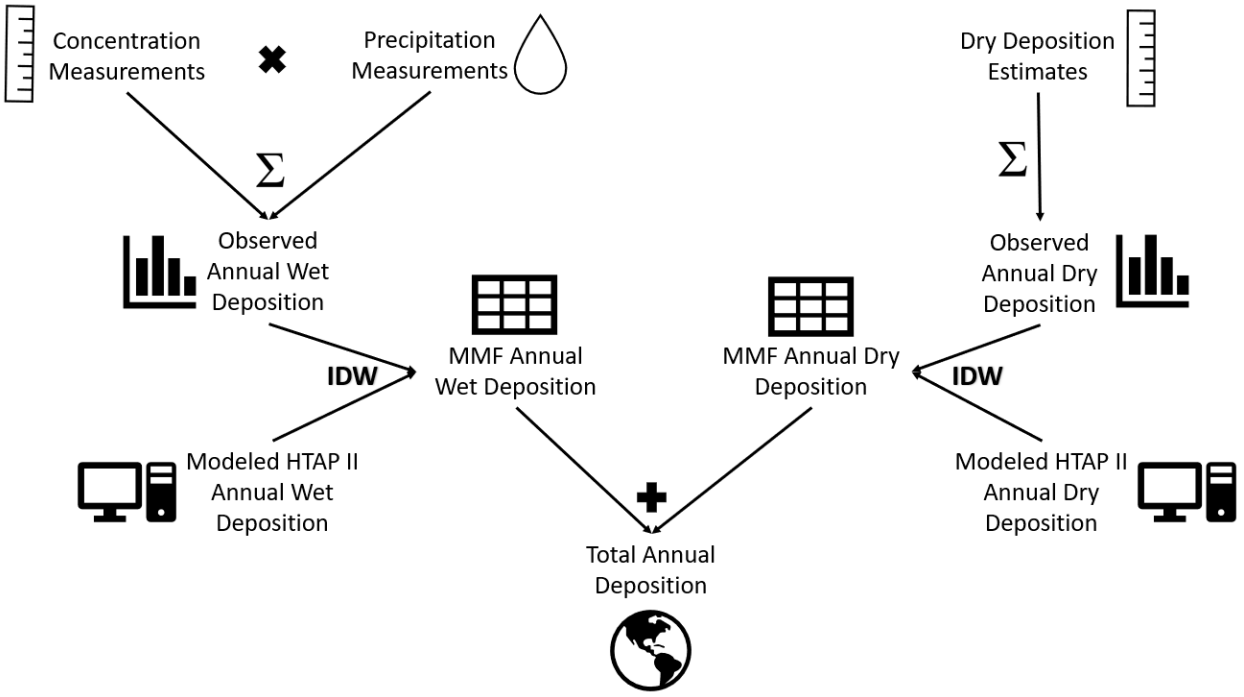

Figure 1. A flowchart describes the MMF methodology implemented in this paper.

4. Results

The total global NH_x deposition in 2010 increased from 54.0 Tg-N (from HTAP II models) to 54.9 Tg-N (Table 2). Combined with a NO_y deposition of 59.6 Tg-N (from a modeled HTAP II 59.3 Tg-N), the total global deposition is adjusted to 114.5Tg-N (from 113 Tg-N), an increase by 1 %. While the IDW tends to decrease the depositions over the continents, an increase is calculated over coastal regions and open oceans using the 2.5x2.5 maximum distance. Total S deposition is adjusted to 88.91 Tg-S (Table 2), an increase by 6.5 % from the HTAP II model prediction of 83.5 Tg-S (Figure 2B). Regional changes greater than or equal to 10% are bolded and italicized.

Table 2: 2010 adjusted global wet and dry deposition in Tg N or Tg S, MMM indicates Tan et al.'s 2018 multi-model mean and MMF is this measurement-model fusion work with a 2.5º interpolation distance. The 1º and 5º interpolation distance results are shown in Tables S1 and S2. Coastal means deposition on sea within 1 degree of the coastline. RBU is an abbreviation for Russia, Belarus, and Ukraine. Open ocean does not include near-land "coastal" waters. The regions can be seen in the world map in Figure S1. Regional changes greater than or equal to 10% are bolded and italicized.

	Non-Coastal		Coastal		Non-Coastal		Coastal		Non-Coastal		Coastal	
	MMM	MMF	MMM	MMF	MMM	MMF	MMM	MMF	MMM	MMF	MMM	MMF
Region	**Total NH_x**				**Total NO_y**				**Total SO_x**			
North America	3.40	3.66	0.40	***0.31***	4.40	4.50	0.80	***0.94***	4.70	**5.67**	1.30	***1.69***
Europe	2.50	2.68	0.80	***1.14***	2.60	2.42	1.20	***1.75***	2.70	2.50	1.50	***3.18***
South Asia	8.60	8.60	1.00	1.00	3.60	3.60	0.70	0.70	3.70	3.70	1.00	1.00
East Asia	6.70	6.49	1.00	1.04	8.30	6.90	2.20	***2.45***	11.20	11.89	2.90	***4.10***
Southeast Asia	3.20	***2.22***	1.60	***2.12***	1.90	***1.60***	1.40	1.44	2.40	***0.81***	2.80	***0.56***
Australia	0.40	0.40	0.40	0.40	0.60	0.60	0.40	0.40	1.00	1.00	1.50	1.50
North Africa	0.70	0.70	0.20	0.20	1.40	1.40	0.40	0.40	1.00	1.00	0.50	0.50
Sub-Saharan Africa	3.40	3.40	0.40	0.40	4.70	4.70	0.60	0.60	2.70	2.70	0.70	0.70
Middle East	0.50	***0.38***	0.10	0.10	1.40	1.31	0.30	0.30	1.70	***3.18***	0.60	0.60
Central America	1.40	1.40	0.60	0.60	1.20	1.20	0.80	0.80	1.40	1.40	1.40	1.40
South America	3.80	3.80	0.30	0.30	3.40	3.40	0.30	0.30	2.40	2.40	0.60	0.60
RBU	1.80	***1.18***	0.30	***0.08***	2.40	***1.36***	0.50	0.47	3.60	***5.10***	0.90	***1.17***
Central Asia	0.50	***0.32***	0.00	0.00	0.60	0.55	0.00	0.00	1.20	***1.88***	0.10	0.10
Antarctica	0.10	0.10	0.00	0.00	0.10	0.10	0.00	0.00	1.40	1.40	0.00	0.00
Continental	37.00	35.33	7.10	7.69	36.70	33.64	9.70	10.55	41.00	44.63	15.60	***17.10***
Open Oceans	9.90	11.86			12.90	15.43			26.90	27.18		
Global	46.90	47.19	7.10	7.69	49.60	49.07	9.70	10.55	67.90	71.81	15.60	***17.10***

191

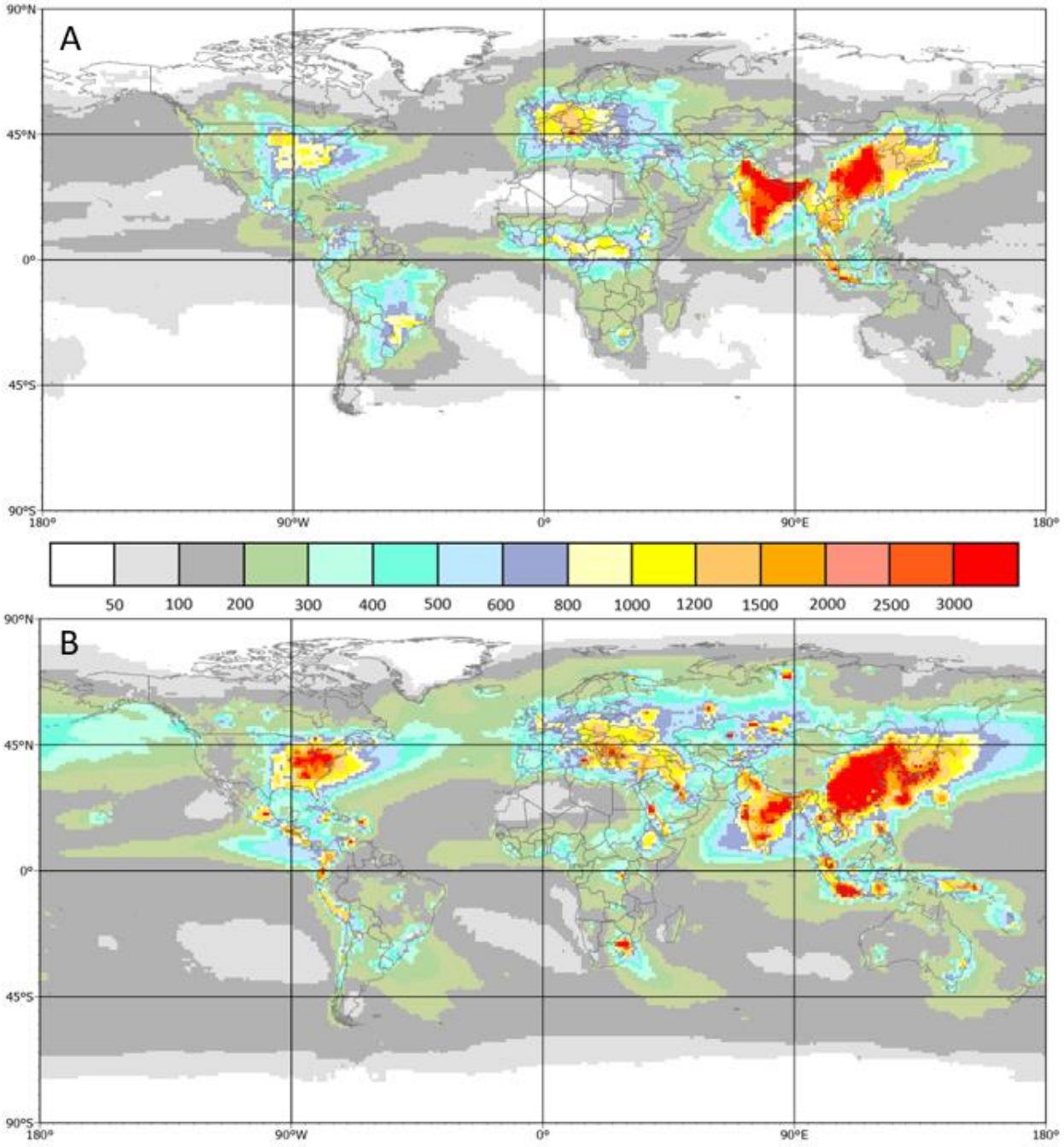

Figure 2: Total N and S deposition in 2010 using the MMF approach. A) Total annual N deposition (mg N/m^2), the sum of wet and dry NO_3^- and NH_4^+ after applying the MMF approach, as well as HTAP II gridded surfaces of dry deposition of NH_3, HNO_3, and NO_2 with no MMF adjustment due to the lack of measurements. **B)** Total S deposition (mg S $/m^2$), the sum of wet and dry MMF SO_4^{2-} and wet and dry HTAP II SO_2.

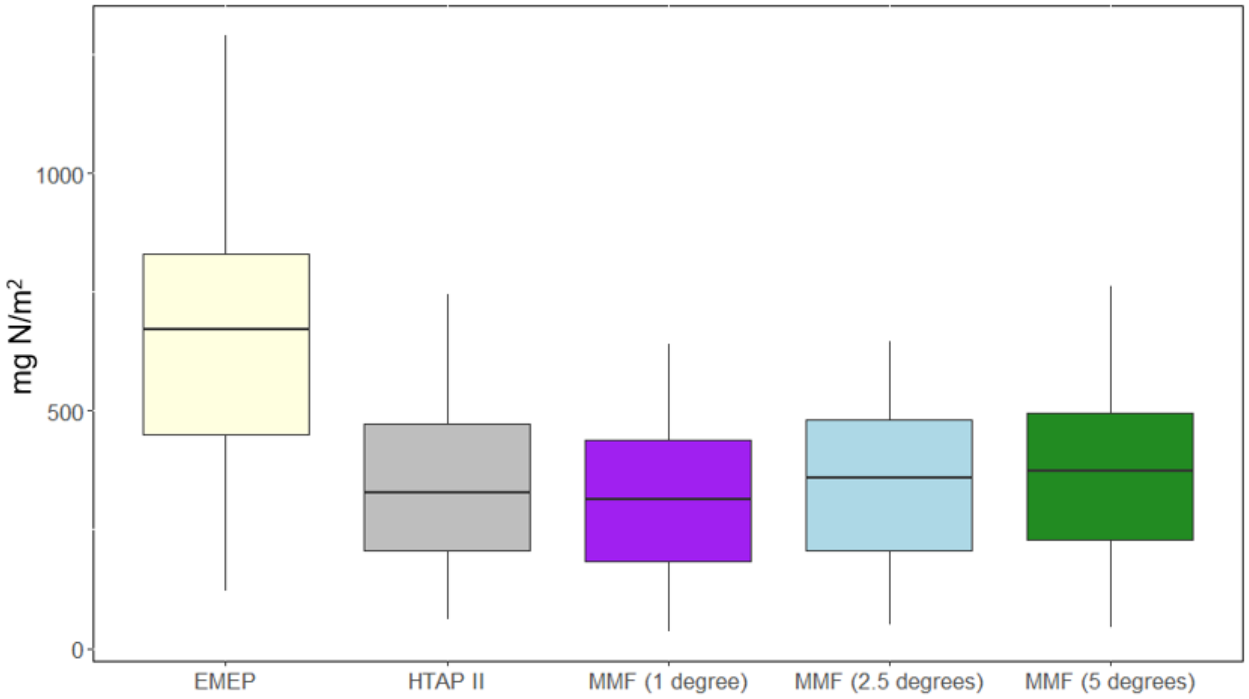

Figure 3: A comparison between HTAP II, MMF, and EMEP wet deposition fluxes in Europe results at EMEP observation sites. A boxplot shows the distribution of EMEP, HTAP II, and MMF modeled wet reactive nitrogen deposition (NH_x and NO_y) results at each EMEP observation location. Three different interpolation distances are compared using MMF, 1 degree, 2.5 degrees, and 5 degrees.

Tan et al. (2018) report that their MMM underestimates the high observations of total N deposition at some EMEP stations in Europe. We find that our 2.5º interpolation value for European wet N deposition (8.0 Tg) is increased by 12.5% relative to the MMM surface (7.1 Tg), although the distance to the observations remains high (Figure 3). Figures 4, S4 and S5 show the difference between HTAP-II MMM and MMF nitrogen and sulfur deposition in North America, Europe, and Asia in mg/m^2 with different interpolation distances. As the interpolation distance increases, locations with a single measurement that is very different from the model will influence the surrounding grid cells to be higher than the model. This effect is in particular pronounced for sulfur deposition in Southeast Asia (Figure 4 B3) where the MMF procedure increases deposition by up to 250 mg/m^2 relative to the MMM values.

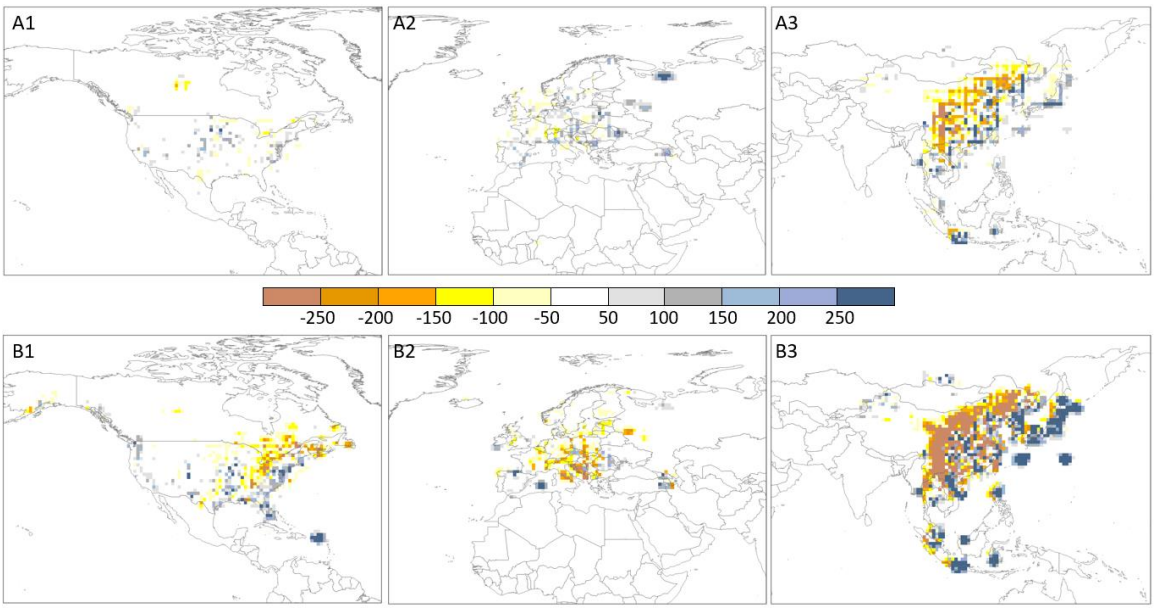

Figure 4. The difference between MMF and MMM deposition with a 2.5-degree interpolation distance. **A)** MMF minus MMM reactive nitrogen deposition in North America (**A1**) Europe (**A2**) and East Asia (**A3**) in mg N/m^2. **B**) MMF minus MMM sulfate deposition in North America (**B1**) Europe (**B2**) and East Asia (**B3**) in mg S/m^2. Results for other interpolation distances are shown in Figures S4 and S5, respectively.

The spatial distribution is slightly different, with more deposition in coastal areas in the MMF estimate (Table 2). Tan et al. (2018) report that the HTAP II MMM overestimates NO_3^- wet deposition in North America, but underestimates NH_4^+ deposition. We find that the MMF interpolated deposition slightly improves these estimates, although the spatial distribution is very similar with the MMM (Figures 2, 5). The largest change for S deposition (comparing MMM and MMF) is in grid cells classified as ocean because of an increase in East and Southeast Asia deposition which mostly occurs in areas classified as ocean due to the small island size relative to the coarse spatial resolution of the models. We note that, ocean cells were classified as such if they were located further than 1º from the mainland; therefore, any islands smaller than 1º were counted as the ocean.

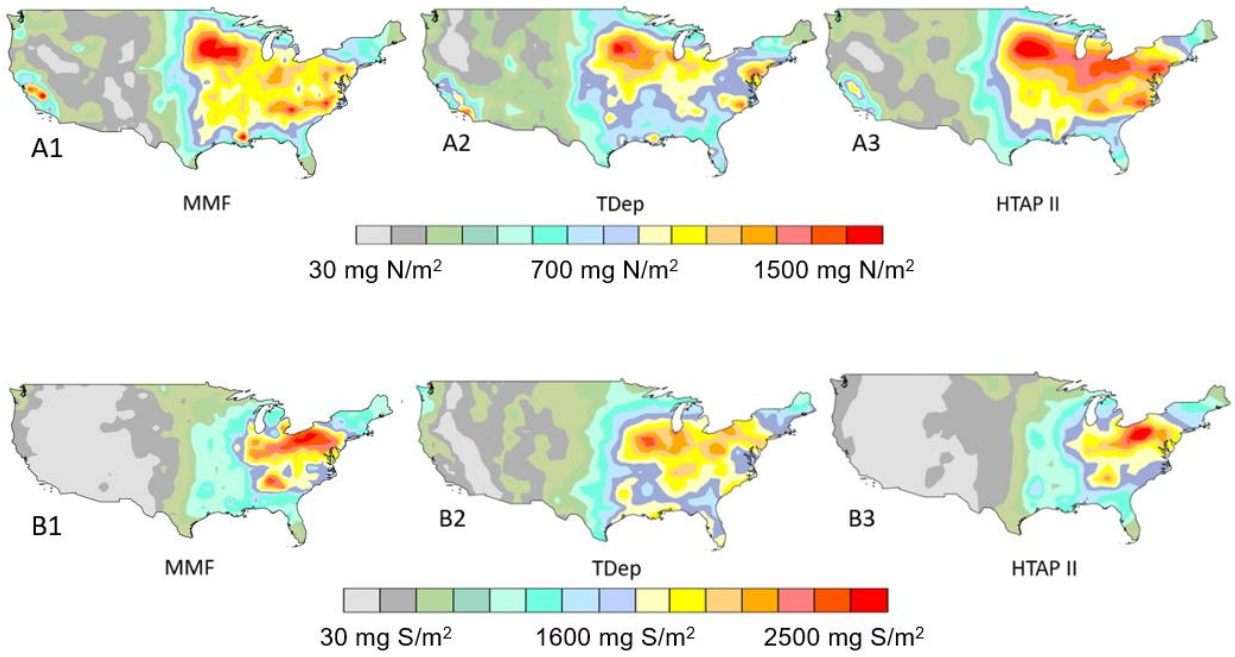

231

232 **Figure 5: 2010 Total N deposition in the continental USA**. **A**) Total N is modeled with 1) MMF (this work), 2)
233 TDep annual map available from the NADP and 3) Tan et al.'s 2018 MMM. **B)** 2010 SO_x wet deposition in the US
234 as modeled with 1) MMF (this work), 2) TDep annual map available from the NADP, and 3) Tan et al.'s 2018
235 multi-model mean HTAP II output.

236

237 There are spatial differences between an aggregated 1º x 1º version of the original TDep map of
238 nitrogen deposition for the United States as available from the NADP (Figure 5A2), the HTAP II
239 (Figure 5A3) deposition produced by Tan et al. (2018) corresponding to the same area, and the
240 deposition map produced in this work (Figure 5A1). A similar pattern is seen in the map of SO_4^{2-}
241 deposition (Figure 5B1; 5B3;5B3). While the TDep maps have been aggregated to the 1x1
242 degree resolution of the HTAP fields, there is still different regional variation in the deposition
243 patterns in the TDep maps than the HTAP II maps. In particular, TDep is capturing higher west
244 coast values that HTAP II does not while showing lower values in the Midwest/New
245 York/Pennsylvania region.

246 The R^2 value for the linear regression between MMF wet SO_4^{2-} and observed wet SO_4^{2-} in the US
247 is 0.64 (Figure 6). The R^2 value for the linear regression between the HTAP II wet SO_4^{2-} and
248 observed SO_4^{2-} is 0.0.60, and 0.89 for the linear regression between the TDep wet SO_4^{2-} and
249 observed SO_4^{2-} (Figure 6). This means that TDep is better reproducing the NADP/NTN

measurements and their spatial differences, whereas the MMF fields remain more similar to the HTAP II ensemble model output. The higher TDep R^2 value likely occurs because of the finer mesh (12 km) used in the TDep product, the closer proximity to individual stations as compared to HTAP II used in the MMF approach, and the ability of the regional model to capture gradients. In principle, emissions should be the same but in global models they are averaged over larger areas. All three datasets produce similar values to the measured wet SO_x deposition at the NADP/NTN sites (Figure 6). The NH_4 and NO_3 wet deposition values are shown in Figures S2 and S3, and have much lower correlations (for all three interpolation distances), with an R^2 of 0.1 for NO_3 and 0.53 for NH_4 at a 2.5º weighted distance

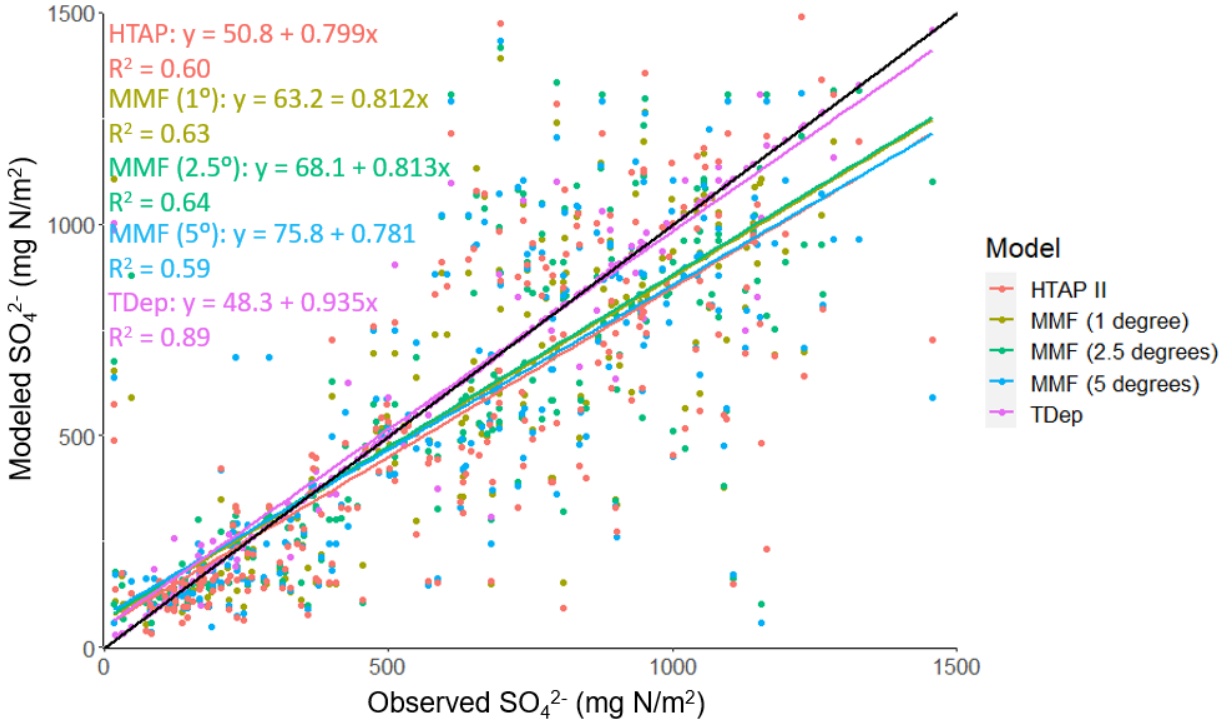

Figure 6: **Observed and modeled wet SO_4^{2-} deposition in the US in 2010**. Each NADP/NTN wet deposition measurement and the associated HTAP II, TDep, or MMF NH_x wet deposition modeled value, with all values shown together in A. The black line is the 1:1 line. Similar plots are shown in Figures S2 and S3 for wet NO_3 and wet NH_4.

5. Discussion

5.1 Consistency of MMF deposition with global emission estimates.

Geddes et al. (2017) used satellite observations to report global NO_y emissions of 57.5 Tg-N/yr in 2010, similar to the 60.4 Tg-N emissions reported by HTAP II. This matches well with our total global MMF-derived NO_y deposition (58.1 Tg-N). HTAP II ammonia emissions were 59.3 Tg-N, slightly lower than the MMF NH_3 and NH_4+ deposition of 62.3 Tg-N. The total MMM sulfur emissions for 2010 were 90.7 Tg S, very similar to the MMF sulfur deposition of 88.9 Tg-N.

5.2 Deposition over China.

A promising data set of wet deposition measurements (NO_3^-, NH_4^+, and SO_4^{2-}) in China is available through the National Nitrogen Deposition Monitoring Network (NNDMN (Xu et al., 2019)). It is comparable to other regional measurements (Wen et al., 2020). However, these data only exist for a fraction of 2010 (from September onwards) for a few sites; rather than use partial data to represent an entire year, these sites were not included in our study. Research in China (Liu et al., 2020) analyzed the spatial pattern of N deposition by combining satellite observations with NNDMN deposition measurements (Xu et al., 2019); they found a 2012 average of 18.21 kg N ha^{-1} for China? Additional work combining the GEOS-Chem (http://acmg.seas.harvard.edu/geos/) model with satellite observations and surface measurements reports the average annual deposition from 2008-2012 as 16.4 Tg-N with 10.2 Tg-N from NH_x and 6.2 Tg-N from NO_y (Zhao et al., 2017). The averages reported by these studies are consistent with ours (16.9 kg ha^{-1} yr^{-1}) despite the difference in year and spatial resolution. The spatial pattern of N deposition in 2010 (Figure 2A) also remains similar to that of previous decades (Jia et al., 2014), with high deposition in eastern China and low deposition over the Tibetan Plateau. This pattern is confirmed in 2006 and 2013 (Qu et al., 2017).

5.3 Limitations of interpolation

As seen in Table 2, the largest difference between MMM and MMF is found in coastal regions and particularly the open ocean. While MMF does give improved deposition estimates by incorporating in-situ measurements, it is worth considering the scale of the model. Observations of deposition are probably not everywhere representative for a 1º or larger resolution and observations of precipitation may also not be homogenous in all directions at that scale, especially over heterogeneous terrain. So, for example, the coarse resolution of the model, even with added measurements is likely not accurately capturing gradients between coastal and inland

deposition. While higher resolution precipitation values are available in some regions (e.g., PRISM in the US), there is still a dearth of both wet and dry deposition measurements. Even on the North American continental scale, Schwede et al. (2011) showed that partially overlapping dry deposition estimates from CASTNET (USA) and CAPMoN (Canada)can be very different, despite using similar methodologies. This adds uncertainty to the dry deposition data (though there are very few dry deposition estimates included in this study) and emphasizes the importance of understanding deposition velocity model methodology.

The differences between the TDep, MMM, and MMF gridded deposition (Figure 5) are clearly visible in the center of the US. While the general patterns of deposition are similar for the three products, the magnitude of deposition in the aggregated TDep dataset (1^{o} x 1^{o}) is higher in the eastern US and lower in the western US than either of the other two deposition fields. This difference is likely due to the precipitation dataset used to calculate wet deposition. The MMF deposition is based on the MMM dataset; therefore, both utilize the same precipitation dataset, from a combination of 11 global models. However, TDep wet deposition is produced by multiplying PRISM precipitation data and an interpolated gridded surface dataset of wet NH_4^+ concentrations. PRISM is a reanalysis product designed to interpolate precipitation in particularly complex landscapes using weather radar and rainfall gauge observations, though it is not identical to observations because it used long-term averages as predictor grids (Zhang et al., 2018). It captures much more localized variation in precipitation due to geographical variations which are not captured in the lower resolution global precipitation models used in the HTAP II MMM (Tan et al., 2018a). To illustrate this, we compare PRISM to the available Community Atmosphere Model with Chemistry (https://www2.acom.ucar.edu/gcm/cam-chem, "CAM-Chem"), which was one of the models in the HTAP II ensemble. Subtracting the CAM-Chem precipitation output over the US from aggregated PRISM precipitation shows that CAM-Chem greatly underestimates precipitation volume in the US in 2010 (Figure S6). We note, however, that this comparison does not take differences in precipitation frequency between the model and observations into account. This matters because if the difference in precipitation volume comes from a few large magnitude storms, it will not influence the overall wet deposition values much. This is a good example of the differences that occur when comparing global and regional climate models and serves to emphasize the importance of resolving spatial and temporal scales. The

total deposition within the US borders is similar for the MMF, HTAP II, and aggregated TDep gridded surfaces; however, the spatial distribution is different.

MMF and MMM deposition distributions are similar because MMF is based on HTAP II. Likewise, the MMF results are similar to the TDep values at observation locations because, despite the difference in precipitation, both utilize the same NADP/NTN measurements to constrain the models. The key difference between MMF, when compared to MMM, is that measurement locations are not centered in each 1º x 1º grid cell; therefore, the center of each grid cell (the value compared to the observation, by interpolation to the station location) will not exactly equal the measured deposition but will instead be equal to the measurements weighted proportionally to distance from the centroid. This means that the graphical comparison of Figure 6 is showing the actual measurement locations and 3 different model results with some meaningful influence from measurements that are nonetheless unique values, except in the very rare instance that the measurement corresponds exactly to the center of a grid cell. Figure 6 shows a stronger correlation for SO_4 than Figures S2 and S3 do for the nitrogen species. This could be related to the relatively shorter timescales of NO_y and NH_x in the atmosphere. The relatively coarse resolution of the global models cannot deal with these gradients, so the shorter timescales are reflected in the observations which are therefore less representative for the larger grid scales of the models.

TDep maps of North American nitrogen deposition created with Schwede and Lear's methodology (2014), using IDW, are widely in use and freely available from the NADP. The sensitivity analysis demonstrates that as the interpolation distance increases, the influence of the observations on the HTAP II grid increases, smoothing some of the artifacts that can occur using a small interpolation distance (Figures 6, S2, S3). In this respect it is worth mentioning that the original TDep dataset for North America used a maximum distance of 30 km plus half the cell size of PRISM (2.07 km). While it is not entirely clear how this distance was determined, operational factors such as the station density and the grid size of the regional model are likely important factors. In contrast, the maximum distances explored in this study are much larger (1º, 2.5º, 5º) and are more adapted to the grid size of the current generation of global atmospheric chemistry transport models, and considerations of transport distances of atmospheric components. From our analysis there is no obvious better weighting distance that improves the comparison with observations. An adaptive distance weighting that considers the expected

gradients between the observation point and the remote model grid could be explored as a way forward.

However, there are strong limitations associated with using IDW (Sahu et al., 2010), and other interpolation methods such as kriging or geographically weighted regression could provide smoother surfaces with fewer artifacts. IDW is a fast and flexible interpolation method, but it does not minimize error and can produce inaccurate results in regions with sparse measurements and large sub-grid variability. This problem is relevant to much of the world. The lack of measurement sites globally is a hindrance that can be alleviated by including information obtained from satellite remote sensing (Walker et al., 2019). Future work should also investigate methods such as machine learning techniques with spatial information to avoid these limitations.

These results from measurement-model fusion are important because previous methods on a global scale have relied primarily on models (Vet et al., 2014; Tan et al., 2018a). They compare their results with measurements, of course, in order to demonstrate the model capabilities but they do not explicitly incorporate point measurements into the final product. Our results serve to emphasize that global models are adequately simulating deposition (in terms of total deposition budgets) but that the regional discrepancies between models and measurements can still be quite large; and measurement-model fusion helps to ameliorate this without changing the fundamental model parameters and processes that actually capture the overall deposition reasonably well.

6. Conclusions

Sulfur and nitrogen deposition remain a serious concern for human and ecosystem health. We update the 2010 deposition budgets using measurement-model fusion to combine the broad spatial coverage of a model with accurate in-situ measurements. The total nitrogen deposition budget is recalculated to 114.50 Tg-N and the sulfur budget is recalculated to 88.91 Tg-N, representing about a 1% and 6.5% increase, respectively, from the modelled values. This work emphasizes the necessity of combining models with observations wherever possible, to better capture regional patterns and to inform policy and decision-making. Future work to improve measurement-model fusion should investigate more advanced MMF methods to avoid the limitations associated with IDW such as surface artifacts and high error in regions with sparse measurements. It could also incorporate satellite remote sensing derived concentrations to

improve model estimates where in-situ measurements are not available, but a careful error analysis is needed to avoid spurious results.

Author Contribution

HR carried out the methods and analyzed the results. JSF and FD designed the project. HR prepared the manuscript with contributions from JSF and FD. RL, KH, and HF provided data.

Competing Interests

The authors declare no competing interests.

Code Availability

Data analysis was done using ArcMap Desktop 10.8.1, ArcGIS Pro, and R (R Core Team, 2022).

References

Adon, M., Galy-Lacaux, C., Yoboué, V., Delon, C., Lacaux, J. P., Castera, P., Gardrat, E., Pienaar, J., Al Ourabi, H., Laouali, D., Diop, B., Sigha-Nkamdjou, L., Akpo, A., Tathy, J. P., Lavenu, F., and Mougin, E.: Long term measurements of sulfur dioxide, nitrogen dioxide, ammonia, nitric acid and ozone in Africa using passive samplers, Atmos. Chem. Phys., 10, 7467–7487, https://doi.org/10.5194/acp-10-7467-2010, 2010.

Anderson, D. M., Burkholder, J. M., Cochlan, W. P., Glibert, P. M., Gobler, C. J., Heil, C. A., Kudela, R. M., Parsons, M. L., Rensel, J. E. J., Townsend, D. W., Trainer, V. L., and Vargo, G. A.: Harmful algal blooms and eutrophication: Examining linkages from selected coastal regions of the United States, Harmful Algae, 8, 39–53, https://doi.org/10.1016/j.hal.2008.08.017, 2008.

Acid Deposition Monitoring Network in East Asia (EANET): https://www.eanet.asia/, last access: 18 November 2021.

Bobbink, R., Hicks, K., Galloway, J., Spranger, T., Alkemade, R., Ashmore, M., Bustamante, M., Cinderby, S., Davidson, E., Dentener, F., Emmett, B., Erisman, J.-W., Fenn, M., Gilliam, F., Nordin, A., Pardo, L., and Vries, W. D.: Global assessment of nitrogen deposition effects on terrestrial plant diversity: a synthesis, Ecological Applications, 20, 30–59, https://doi.org/10.1890/08-1140.1, 2010.

Bowman, W. D., Cleveland, C. C., Halada, Ĺ., Hreško, J., and Baron, J. S.: Negative impact of nitrogen deposition on soil buffering capacity, Nature Geoscience, 1, 767–770, https://doi.org/10.1038/ngeo339, 2008.

Clark, C. M., Bai, Y., Bowman, W. D., Cowles, J. M., Fenn, M. E., Gilliam, F. S., Phoenix, G. K., Siddique, I., Stevens, C. J., Sverdrup, H. U., and Throop, H. L.: Nitrogen Deposition and Terrestrial Biodiversity, in: Encyclopedia of Biodiversity, Elsevier, 519–536, https://doi.org/10.1016/B978-0-12-384719-5.00366-X, 2013.

Dentener, F., Drevet, J., Lamarque, J. F., Bey, I., Eickhout, B., Fiore, A. M., Hauglustaine, D., Horowitz, L. W., Krol, M., Kulshrestha, U. C., Lawrence, M., Galy-Lacaux, C., Rast, S., Shindell, D., Stevenson, D., Noije, T. V., Atherton, C., Bell, N., Bergman, D., Butler, T., Cofala, J., Collins, B., Doherty, R., Ellingsen, K., Galloway, J., Gauss, M., Montanaro, V., Müller, J. F., Pitari, G., Rodriguez, J., Sanderson, M., Solmon, F., Strahan, S., Schultz, M., Sudo, K., Szopa, S., and Wild, O.: Nitrogen and sulfur deposition on regional and global scales: A multimodel evaluation, Global Biogeochemical Cycles, 20, https://doi.org/10.1029/2005GB002672, 2006.

Dise, N. B. and Stevens, J.: Nitrogen deposition and reduction of terrestrial biodiversity: Evidence from temperate grasslands, Sci. China Ser. C.-Life Sci., 48, 720–728, https://doi.org/10.1007/BF03187112, 2005.

Doney, S. C., Mahowald, N., Lima, I., Feely, R. A., Mackenzie, F. T., Lamarque, J.-F., and Rasch, P. J.: Impact of anthropogenic atmospheric nitrogen and sulfur deposition on ocean acidification and the inorganic carbon system, PNAS, 104, 14580–14585, https://doi.org/10.1073/pnas.0702218104, 2007.

European Monitoring and Evaluation Prgrarmme (EMEP): https://www.emep.int/, last access: 18 November 2021.

Canadian Air and Precipitation Monitoring Network: https://www.canada.ca/en/environment-climate-change/services/air-pollution/monitoring-networks-data/canadian-air-precipitation.html, last access: 18 November 2021.

Fu, J. S., Carmichael, G. R., Dentener, F., Aas, W., Andersson, C., Barrie, L. A., Cole, A., Galy-Lacaux, C., Geddes, J., Itahashi, S., Kanakidou, M., Labrador, L., Paulot, F., Schwede, D., Tan, J., and Vet, R.: Improving Estimates of Sulfur, Nitrogen, and Ozone Total Deposition through Multi-Model and Measurement-Model Fusion Approaches, Environ. Sci. Technol., 56, 2134–2142, https://doi.org/10.1021/acs.est.1c05929, 2022.

Galy-Lacaux, C., Delon, C., Solmon, F., Adon, M., Yoboué, V., Mphepya, J., Pienaar, J. J., Diop, B., Sigha, L., Dungall, L., Akpo, A., Mougin, E., Gardrat, E., and Castera, P.: Dry and Wet Atmospheric Nitrogen Deposition in West Central Africa, in: Nitrogen Deposition, Critical Loads and Biodiversity, edited by: Sutton, M. A., Mason, K. E., Sheppard, L. J., Sverdrup, H., Haeuber, R., and Hicks, W. K., Springer Netherlands, Dordrecht, 83–91, https://doi.org/10.1007/978-94-007-7939-6_10, 2014.

Geddes, J. A. and Martin, R. V.: Global deposition of total reactive nitrogen oxides from 1996 to 2014 constrained with satellite observations of NO_2 columns, Atmospheric Chemistry and Physics, 17, 10071–10091, https://doi.org/10.5194/acp-17-10071-2017, 2017.

Heisler, J., Glibert, P. M., Burkholder, J. M., Anderson, D. M., Cochlan, W., Dennison, W. C., Dortch, Q., Gobler, C. J., Heil, C. A., Humphries, E., Lewitus, A., Magnien, R., Marshall, H. G., Sellner, K., Stockwell, D. A., Stoecker, D. K., and Suddleson, M.: Eutrophication and harmful algal blooms: A scientific consensus, Harmful Algae, 8, 3–13, https://doi.org/10.1016/j.hal.2008.08.006, 2008.

INDAAF – International Network to study Deposition and Atmospheric chemistry in AFrica: https://indaaf.obs-mip.fr/, last access: 18 November 2021.

Jia, Y., Yu, G., He, N., Zhan, X., Fang, H., Sheng, W., Zuo, Y., Zhang, D., and Wang, Q.: Spatial and decadal variations in inorganic nitrogen wet deposition in China induced by human activity, Sci Rep, 4, 3763, https://doi.org/10.1038/srep03763, 2014.

Kicklighter, D. W., Melillo, J. M., Monier, E., Sokolov, A. P., and Zhuang, Q.: Future nitrogen availability and its effect on carbon sequestration in Northern Eurasia, Nat Commun, 10, 3024, https://doi.org/10.1038/s41467-019-10944-0, 2019.

Labrador, L., Volosciuk, C., and Cole, A.: Measurement-Model Fusion for Global Total Atmospheric Deposition, a WMO initiative, World Meteorological Organization, 2020.

Lamarque, J.-F., Dentener, F., McConnell, J., Ro, C.-U., Shaw, M., Vet, R., Bergmann, D., Cameron-Smith, P., Dalsoren, S., Doherty, R., Faluvegi, G., Ghan, S. J., Josse, B., Lee, Y. H., MacKenzie, I. A., Plummer, D., Shindell, D. T., Skeie, R. B., Stevenson, D. S., Strode, S., Zeng, G., Curran, M., Dahl-Jensen, D., Das, S., Fritzsche, D., and Nolan, M.: Multi-model mean

nitrogen and sulfur deposition from the Atmospheric Chemistry and Climate Model Intercomparison Project (ACCMIP): evaluation of historical and projected future changes, Atmos. Chem. Phys., 13, 7997–8018, https://doi.org/10.5194/acp-13-7997-2013, 2013.

Li, R., Cui, L., Zhao, Y., Zhang, Z., Sun, T., Li, J., Zhou, W., Meng, Y., Huang, K., and Fu, H.: Wet deposition of inorganic ions in 320 cities across China: spatio-temporal variation, source apportionment, and dominant factors, Atmospheric Chemistry and Physics, 19, 11043–11070, https://doi.org/10.5194/acp-19-11043-2019, 2019.

Liu, L., Zhang, X., Xu, W., Liu, X., Zhang, Y., Li, Y., Wei, J., Lu, X., Wang, S., Zhang, W., Zhao, L., Wang, Z., and Wu, X.: Fall of oxidized while rise of reduced reactive nitrogen deposition in China, Journal of Cleaner Production, 272, 122875, https://doi.org/10.1016/j.jclepro.2020.122875, 2020.

Lu, Z., Streets, D. G., Zhang, Q., Wang, S., Carmichael, G. R., Cheng, Y. F., Wei, C., Chin, M., Diehl, T., and Tan, Q.: Sulfur dioxide emissions in China and sulfur trends in East Asia since 2000, Atmos. Chem. Phys., 10, 6311–6331, https://doi.org/10.5194/acp-10-6311-2010, 2010.

Luo, X. S., Tang, A. H., Shi, K., Wu, L. H., Li, W. Q., Shi, W. Q., Shi, X. K., Erisman, J. W., Zhang, F. S., and Liu, X. J.: Chinese coastal seas are facing heavy atmospheric nitrogen deposition, Environ. Res. Lett., 9, 095007, https://doi.org/10.1088/1748-9326/9/9/095007, 2014.

National Atmospheric Deposition Program: https://nadp.slh.wisc.edu/, last access: 18 November 2021.

Qu, L., Xiao, H., Zheng, N., Zhang, Z., and Xu, Y.: Comparison of four methods for spatial interpolation of estimated atmospheric nitrogen deposition in South China, Environ Sci Pollut Res, 24, 2578–2588, https://doi.org/10.1007/s11356-016-7995-0, 2017.

R Core Team: R: A Language and Environment for Statistical Computing, 2022.

Sahu, S. K., Gelfand, A. E., and Holland, D. M.: Fusing point and areal level space–time data with application to wet deposition, Journal of the Royal Statistical Society: Series C (Applied Statistics), 59, 77–103, https://doi.org/10.1111/j.1467-9876.2009.00685.x, 2010.

Schwede, D., Zhang, L., Vet, R., and Lear, G.: An intercomparison of the deposition models used in the CASTNET and CAPMoN networks, Atmospheric Environment, 45, 1337–1346, https://doi.org/10.1016/j.atmosenv.2010.11.050, 2011.

Schwede, D., Cole, A., Vet, R., and Lear, G.: Ongoing U.S. - Canada Collaboration on Nitrogen and Sulfur Deposition, 5, 2019.

Schwede, D. B. and Lear, G. G.: A novel hybrid approach for estimating total deposition in the United States, Atmospheric Environment, 92, 207–220, https://doi.org/10.1016/j.atmosenv.2014.04.008, 2014.

Sirois, A.: The effects of missing data on the calculation of precipitation-weighted-mean concentrations in wet deposition, Atmospheric Environment. Part A. General Topics, 24, 2277–2288, https://doi.org/10.1016/0960-1686(90)90321-D, 1990.

Tan, J., Fu, J. S., Dentener, F., Sun, J., Emmons, L., Tilmes, S., Sudo, K., Flemming, J., Jonson, J. E., Gravel, S., Bian, H., Davila, Y., Henze, D. K., Lund, M. T., Kucsera, T., Takemura, T., and Keating, T.: Multi-model study of HTAP II on sulfur and nitrogen deposition, Atmospheric Chemistry and Physics, 18, 6847–6866, https://doi.org/10.5194/acp-18-6847-2018, 2018a.

Tan, J., Fu, J. S., Dentener, F., Sun, J., Emmons, L., Tilmes, S., Flemming, J., Takemura, T., Bian, H., Zhu, Q., Yang, C.-E., and Keating, T.: Source contributions to sulfur and nitrogen deposition – an HTAP II multi-model study on hemispheric transport, Atmospheric Chemistry and Physics, 18, 12223–12240, https://doi.org/10.5194/acp-18-12223-2018, 2018b.

Tørseth, K., Aas, W., Breivik, K., Fjæraa, A. M., Fiebig, M., Hjellbrekke, A. G., Lund Myhre, C., Solberg, S., and Yttri, K. E.: Introduction to the European Monitoring and Evaluation Programme (EMEP) and observed atmospheric composition change during 1972 - 2009, Atmospheric Chemistry and Physics, 12, 5447–5481, https://doi.org/10.5194/acp-12-5447-2012, 2012.

Clean Air Status and Trends Network (CASTNET): https://www.epa.gov/castnet, last access: 18 November 2021.

Vet, R., Artz, R. S., Carou, S., Shaw, M., Ro, C.-U., Aas, W., Baker, A., Bowersox, V. C., Dentener, F., Galy-Lacaux, C., Hou, A., Pienaar, J. J., Gillett, R., Forti, M. C., Gromov, S., Hara, H., Khodzher, T., Mahowald, N. M., Nickovic, S., Rao, P. S. P., and Reid, N. W.: A global assessment of precipitation chemistry and deposition of sulfur, nitrogen, sea salt, base cations, organic acids, acidity and pH, and phosphorus, Atmospheric Environment, 93, 3–100, https://doi.org/10.1016/j.atmosenv.2013.10.060, 2014.

de Vries, W., Solberg, S., Dobbertin, M., Sterba, H., Laubhann, D., van Oijen, M., Evans, C., Gundersen, P., Kros, J., Wamelink, G. W. W., Reinds, G. J., and Sutton, M. A.: The impact of nitrogen deposition on carbon sequestration by European forests and heathlands, Forest Ecology and Management, 258, 1814–1823, https://doi.org/10.1016/j.foreco.2009.02.034, 2009.

Walker, J. T., Beachley, G., Amos, H. M., Baron, J. S., Bash, J., Baumgardner, R., Bell, M. D., Benedict, K. B., Chen, X., Clow, D. W., Cole, A., Coughlin, J. G., Cruz, K., Daly, R. W., Decina, S. M., Elliott, E. M., Fenn, M. E., Ganzeveld, L., Gebhart, K., Isil, S. S., Kerschner, B. M., Larson, R. S., Lavery, T., Lear, G. G., Macy, T., Mast, M. A., Mishoe, K., Morris, K. H., Padgett, P. E., Pouyat, R. V., Puchalski, M., Pye, H. O. T., Rea, A. W., Rhodes, M. F., Rogers, C. M., Saylor, R., Scheffe, R., Schichtel, B. A., Schwede, D. B., Sexstone, G. A., Sive, B. C., Sosa Echeverría, R., Templer, P. H., Thompson, T., Tong, D., Wetherbee, G. A., Whitlow, T. H., Wu, Z., Yu, Z., and Zhang, L.: Toward the improvement of total nitrogen deposition budgets in the United States, Science of The Total Environment, 691, 1328–1352, https://doi.org/10.1016/j.scitotenv.2019.07.058, 2019.

Wen, Z., Xu, W., Li, Q., Han, M., Tang, A., Zhang, Y., Luo, X., Shen, J., Wang, W., Li, K., Pan, Y., Zhang, L., Li, W., Collett, J. L., Zhong, B., Wang, X., Goulding, K., Zhang, F., and Liu, X.:

548 Changes of nitrogen deposition in China from 1980 to 2018, Environment International, 144,
549 106022, https://doi.org/10.1016/j.envint.2020.106022, 2020.

550 Xu, W., Luo, X. S., Pan, Y. P., Zhang, L., Tang, A. H., Shen, J. L., Zhang, Y., Li, K. H., Wu, Q.
551 H., Yang, D. W., Zhang, Y. Y., Xue, J., Li, W. Q., Li, Q. Q., Tang, L., Lu, S. H., Liang, T.,
552 Tong, Y. A., Liu, P., Zhang, Q., Xiong, Z. Q., Shi, X. J., Wu, L. H., Shi, W. Q., Tian, K., Zhong,
553 X. H., Shi, K., Tang, Q. Y., Zhang, L. J., Huang, J. L., He, C. E., Kuang, F. H., Zhu, B., Liu, H.,
554 Jin, X., Xin, Y. J., Shi, X. K., Du, E. Z., Dore, A. J., Tang, S., Collett, J. L., Goulding, K., Sun,
555 Y. X., Ren, J., Zhang, F. S., and Liu, X. J.: Quantifying atmospheric nitrogen deposition through
556 a nationwide monitoring network across China, Atmos. Chem. Phys., 15, 12345–12360,
557 https://doi.org/10.5194/acp-15-12345-2015, 2015.

558 Xu, W., Zhang, L., and Liu, X.: A database of atmospheric nitrogen concentration and deposition
559 from the nationwide monitoring network in China, Sci Data, 6, 51,
560 https://doi.org/10.1038/s41597-019-0061-2, 2019.

561 Zhang, M., Leon, C. de, and Migliaccio, K.: Evaluation and comparison of interpolated gauge
562 rainfall data and gridded rainfall data in Florida, USA, Hydrological Sciences Journal, 63, 561–
563 582, https://doi.org/10.1080/02626667.2018.1444767, 2018.

564 Zhang, Y., Foley, K. M., Schwede, D. B., Bash, J. O., Pinto, J. P., and Dennis, R. L.: A
565 Measurement-Model Fusion Approach for Improved Wet Deposition Maps and Trends, Journal
566 of Geophysical Research: Atmospheres, 124, 4237–4251,
567 https://doi.org/10.1029/2018JD029051, 2019.

568 Zhao, Y., Zhang, L., Chen, Y., Liu, X., Xu, W., Pan, Y., and Duan, L.: Atmospheric nitrogen
569 deposition to China: A model analysis on nitrogen budget and critical load exceedance,
570 Atmospheric Environment, 153, 32–40, https://doi.org/10.1016/j.atmosenv.2017.01.018, 2017.

571 Zhu, J., Chen, Z., Wang, Q., Xu, L., He, N., Jia, Y., Zhang, Q., and Yu, G.: Potential transition in
572 the effects of atmospheric nitrogen deposition in China, Environmental Pollution, 258, 113739,
573 https://doi.org/10.1016/j.envpol.2019.113739, 2020.

574